HHS Public Access

Author manuscript

Mol Neurobiol. Author manuscript; available in PMC 2021 December 01.

Published in final edited form as:

Mol Neurobiol. 2020 December ; 57(12): 5307–5323. doi:10.1007/s12035-020-02092-0.

Combined *Atoh1* and *Neurod1* deletion reveals autonomous growth of auditory nerve fibers

Iva Filova[1], **Martina Dvorakova**[1], **Romana Bohuslavova**[1], **Adam Pavlinek**[1], **Karen E. Thompson**[2], **Simona Vochyanova**[1], **Bernd Fritzsch**[2,*], **Gabriela Pavlinkova**[1,*]

[1]Institute of Biotechnology of the Czech Academy of Sciences, 25250 Vestec, Czechia

[2]Department of Biology, University of Iowa, Iowa City, IA 52242-1324, USA

Abstract

Ear development requires the transcription factors ATOH1 for hair cell differentiation and NEUROD1 for sensory neuron development. In addition, NEUROD1 negatively regulates *Atoh1* gene expression. As we previously showed that deletion of *Neurod1* gene in the cochlea results in guidance defects and excessive peripheral innervation of the sensory epithelium, we hypothesized that some of the innervation defects may be a result of abnormalities in NEUROD1 and ATOH1 interactions. To characterize the interdependency of ATOH1 and NEUROD1 in inner ear development, we generated a new *Atoh1/Neurod1* double null conditional deletion mutant. Through careful comparison of the effects of single *Atoh1* or *Neurod1* gene deletion with combined double *Atoh1* and *Neurod1* deletion, we demonstrate that NEUROD1-ATOH1 interactions are not important for the *Neurod1* null innervation phenotype. We report that neurons lacking *Neurod1* can innervate the flat epithelium without any sensory hair cells or supporting cells left after *Atoh1* deletion, indicating that neurons with *Neurod1* deletion do not require the presence of hair cells for axon growth. Moreover, transcriptome analysis identified genes encoding axon guidance and neurite growth molecules dysregulated in the *Neurod1* deletion mutant. Taken together, we demonstrate that much of the projections of NEUROD1-deprived inner ear sensory neurons are regulated cell-autonomously.

Keywords

bHLH genes; ear neurosensory development; neuronal differentiation; central projections; axon guidance

*the corresponding author (gpavlinkova@ibt.cas.cz) and (bernd-fritzsch@uiowa.edu).

Authors' contributions G.P., B.F. conceptualized the work, and wrote the MS. I.M. wrote the first draft of the paper. I.M., M.D., S.V., K.E.T. and R.B. performed *in situ* hybridization and immunohistological analyses. R.B. prepared and validated RNA for RNA-Seq. A.P. performed qPCR and RNA-Seq bioinformatics analyses and the editing of the MS. B.F. performed dye tracing.

Conflicts of interest/Competing interests The authors declare that they have no conflict of interest.

Ethics approval All methods were performed in agreement with the Guide for the Care and Use of Laboratory Animals (National Research Council. Washington, DC. The National Academies Press, 1996). The design of experiments was approved by the Animal Care and Use Committee of the Institute of Molecular Genetics, Czechia.

Introduction

Ear morphogenesis is governed by a gene regulatory network formed by the temporal and spatial integration of signaling pathways and transcription factors. Neural, sensory, and non-sensory cell fates are defined by regulatory patterns mediated by local interactions (Delta-Notch); morphogen gradients of WNT, FGF, SHH, and BMP signaling [1]; and regionally expressed transcription factors (EYA1, SIX1, GATA3, PAX2, SOX2 [2–5]). The initial neurosensory domain is transformed into distinct cell types by the expression of basic helix-loop-helix (bHLH) transcription factors (ATOH1, NEUROGENIN1, and NEUROD1). Inner ear neuronal development depends on NEUROGENIN1 (NEUROG1) and NEUROD1 for neuronal specification and differentiation, whereas sensory cell fate specification occurs after neurogenesis and is associated with ATOH1 expression [6,7]. NEUROG1, the first bHLH factor upregulated in the inner ear [8], activates downstream *Neurod1* gene expression for neuronal development and survival of most neurons [9]. NEUROD1 provides negative feedback for *Atoh1* by suppressing an alternate ATOH1-mediated hair cell (HC) fate within the ganglia, and delays ATOH1 upregulation and premature HC differentiation in the apex [10,11]. ATOH1 is required for HC differentiation but not for the establishment of sensory precursors that eventually die in *Atoh1* gene deletion mutants [12–14]. Although the decision between neuron and hair cell fate in the inner ear is governed by a mutual antagonism of these bHLH factors [7], the detailed functional and molecular interactions between ATOH1 and NEUROD1 within the emerging transcriptional network of neurosensory development remains unresolved.

We previously demonstrated that $Isl1^{Cre}$-mediated *Neurod1* gene deletion in the inner ear resulted in a disorganized cochleotopic projection from spiral ganglion neurons, affecting the frequency, intensity, and temporal processing in the central auditory system of adult mice at the physiological and behavioral level [15]. As *Neurod1* deletion in the cochlea results in guidance defects and excessive peripheral innervation, we wanted to establish if these innervation defects are a result of abnormalities in ATOH1-NEUROD1 interactions. To study this, we generated a new conditional deletion model of *Atoh1*/*Neurod1* double null mutant mice (*Atoh1/Neurod1CKO)*. Our data demonstrate that neurons lacking *Neurod1* do not require differentiated sensory HCs for axon growth because we find nearly identically disorganized and excessive innervation in double *Atoh1/Neurod1CKO* as in single *Neurod1CKO* mutants.

Materials and Methods

Experimental animals

All methods were performed in agreement with the Guide for the Care and Use of Laboratory Animals (National Research Council. Washington, DC. The National Academies Press, 1996). The design of experiments was approved by the Animal Care and Use Committee of the Institute of Molecular Genetics, Czech Academy of Sciences. The mice were housed in 12-hour light/dark cycles and were fed *ad libitum*. We cross-bred $Isl1^{Cre}$ with a direct *Cre* knockin into the endogenous *Isl1* locus ($Isl1^{Cre}$; $Isl1^{tm1(Cre)Sev}/J$, #024242, The Jackson Laboratory)[16] with two transgenic mouse lines: floxed *Neurod1*

(*Neurod1*$^{loxP/loxP}$)[17] and floxed *Atoh1* (*Atoh1*$^{loxP/loxP}$, #008681, The Jackson Laboratory) [18] to generate mice with the conditional deletion of *Atoh1* (*Atoh1CKO*) and *Neurod1* (*Neurod1CKO*) or double gene deletions (*Atoh1/Neurod1CKO*). Heterozygous animals (*Isl1*^{Cre}*;Neurod1*$^{+/f}$*; Isl1*^{Cre}*;Atoh1*$^{+/f}$) were viable, born in appropriate Mendelian ratios, and were phenotypically indistinguishable from control (Cre negative) littermate mice (*Neurod1*$^{f/f}$, *Neurod1*$^{+/f}$, *Atoh1*$^{f/f}$, and *Atoh1*$^{+/f}$). The double *Atoh1/Neurod1*-deficient embryos (*Atoh1/Neurod1CKO*) were generated by crossing *Isl1*^{Cre}*;Neurod1*$^{+/f}$*;Atoh1*$^{+/f}$ mice to *Atoh1*$^{f/f}$;*Neurod1*$^{f/f}$. The littermate controls for *Atoh1/Neurod1CKO* were embryos with floxed allele genotypes (*Neurod1*$^{+/f}$*, Atoh1*$^{+/f}$*, Atoh1*$^{f/f}$ or *Neurod1*$^{f/f}$). Both males and females were used for experiments. All comparisons were made between animals with the same genetic background, typically littermates. Phenotyping and data analysis were performed blind to the genotype of the mice.

Timed pregnancies and genotyping

The noon of the day the vaginal plug was found was defined as embryonic day 0.5 (E0.5). Embryos and littermates were genotyped using polymerase chain reaction of DNA from tail biopsy. The specific primers used were the following: *Isl1-Cre* F 5'-GCC TGC ATT ACC GGT CGA TGC AAC GA-3' and *Isl1-Cre* R 5'-GTG GCA GAT GGC GCG GCA ACA CCA TT-3' with a 700 bp product; *Atoh1* F 5'-AGC GAT GAT GGC ACA GAA G-3' and *Atoh1* R 5'-GAA GTC AAG TCG TTG CTA AC-3' with a 300 bp product for WT allele or 500 bp product for the floxed allele; *Neurod1* F 5'-ACC ATG CAC TCT GTA CGC ATT-3' and *Neurod1* R 5'-GAG AAC TGA GAC ACT CAT CTG-3' with a 400 bp product for WT allele or 600 bp for the floxed allele.

In situ hybridization

In situ hybridization was performed using an RNA probe labeled with digoxigenin as previously described [19]. The plasmid carrying *Atoh1* cDNA was a gift from H. Zoghbi. Briefly, dissected inner ears freed from cartilage were incubated with Proteinase K (Thermo Fisher Scientific EO0492, 1:1 000) in 1×Phosphate Buffered Saline, pH 7.4 (PBS) for 22 minutes. The samples were incubated overnight in hybridization solution containing 50% (v/v) formamide, 50% (v/v) saline-sodium citrate buffer and 6% (w/v) dextran sulphate, denatured DNA (Sigma-Aldrich 11467140001 ROCHE), and 150 ng/ml *Atoh1* probe at 60°C overnight. Unbound probe was digested using RNase A (Thermo Fisher Scientific EN0531, 1:2 000), and samples were incubated with anti-digoxigenin antibody conjugated with alkaline phosphatase (Sigma-Aldrich 11093274910 ROCHE, 1:2 000) at 4°C overnight. BM-Purple chromogenic substrate (Sigma-Aldrich 11442074001 ROCHE) for alkaline phosphatase was used to visualize bound riboprobes. Stained inner ears were mounted in glycerol and images were taken with a Nikon Eclipse 50i microscope. The *in situ* hybridization was repeated 3x with the different sets of individual control and *Atoh1CKO* samples.

Immunohistochemistry

Embryos were dissected in cold PBS, and embryos or dissected ears were fixed in 4% paraformaldehyde (PFA) in PBS. For vibratome sections, samples were embedded in 4% agarose and sectioned at 80 μm on a Leica VT1000S vibratome. Vibratome sections, whole

inner ears or whole embryos were defatted in 70% ethanol and then rehydrated and blocked with serum, as described previously [19,20]. Samples were then incubated with primary antibodies at 4°C for 72 hours. The primary antibodies used were: rabbit anti-Myosin 7a (Myo7a; Proteus BioSciences 25–6790, 1:500), mouse anti-acetylated α-tubulin (tubulin; Sigma-Aldrich T6793, 1:400), rabbit anti-calretinin (Santa Cruz Biotechnology sc-50453, 1:100), goat anti-prestin (Santa Cruz Biotechnology sc-22692, 1:50), goat anti-SOX2 (Santa Cruz Biotechnology sc-17320, 1:250), rabbit anti-cleaved Caspase-3 (Cell Signaling Technology 9661, 1:100), rabbit anti-NeuN (Abcam ab177487, 1:500), mouse anti-Isl1 (39.3F7, Developmental Hybridoma Bank,1:130), goat anti-Neurod1 (sc-1084, Santa Cruz Biotechnology, 1:100), rabbit anti-Cre (908001, BioLegend, 1:500), and rabbit anti-Prox1 (BioLegend 925201, 1:500). After several PBS washes, secondary antibodies were added and incubated in 4°C for 24 hours. The secondary antibodies Alexa Fluor® 488 AffiniPure Goat Anti-Mouse IgG (Jackson ImmunoResearch Laboratories 115-545-146), Alexa Fluor® 594 AffiniPure Goat Anti-Rabbit IgG (Jackson ImmunoResearch Laboratories 111-585-144) and DyLight488-conjugated AffiniPure Mouse Anti-Goat IgG (Jackson ImmunoResearch Laboratories 205-485-108) were used in 1:400 dilution. Nuclei were stained by Hoechst 33258 (Sigma-Aldrich 861405, 1:2 000). Samples were mounted in Aqua-Poly/Mount (Polysciences 18606) or in prepared Antifade medium and images were taken on Zeiss LSM 5 DUO, Zeiss LSM 880 or Leica SPE confocal microscopes. Image stacks were collected and sets of stacks were combined into the single image. ImageJ and ZEN software were used for image processing. The quantification of tubulin-labeled fibers in the area of the organ of Corti was assessed using the thresholding tool in ImageJ. The length of the cochlea was established using the ImageJ Tool “Measure”. The number of *Neurod1*$^{+}$ cells in the inner ear ganglia was determined by the ImageJ Plugin “Cell Counter”.

X-gal staining

Mice carrying *Isl1*^{Cre} and *R26R-lacZ* (*Gt(ROSA)26Sor*^{tm1Sor}, #003309, The Jackson Laboratory) were anaesthetized and perfused with PBS followed by 4% paraformaldehyde. The inner ears were dissected and processed for X-gal staining, as described previously [19].

Scanning electron microscopy

Inner ears were microdissected, cleansed of membranes to expose the HCs of the organ of Corti. Cochleae were placed in porous specimen pots and were then extensively washed and dehydrated through an alcohol series ending with absolute acetone. Tissues were dried to a critical point in liquid CO_2 in a K 850 unit (Quorum Technologies Ltd, Ringmer, UK). The dried samples were mounted onto carbon conductive double-sided adhesive discs and sputter-coated with 20 nm of gold in a Polaron Sputter-Coater (E5100)(Quorum Technologies Ltd, Ringmer, UK). The final samples were examined in a FEI Nova NanoSem 450 scanning electron microscope (FEI Czech Republic s.r.o.) at 5 kV using a secondary electron detector.

Lipophilic Dye Tracing

The pattern of innervation was evaluated in whole or dissected ears and brains using lipophilic dye tracing in aldehyde fixed tissue as previously described [21]. At least three mutants and similar numbers of control littermates were used for each stage examined

(E16.5, E18.5). We inserted filter strips loaded with different colored lipophilic dyes into the cochlear apex, base, vestibular end organs, cochlear/vestibular nuclei of the brainstem around rhombomere 5 to label afferents, and into rhombomere 4 near the midline to label inner ear efferents [22]. After diffusion of the lipophilic tracer from insertion to target, we prepared the ears or brains as whole mounts, mounted with glycerol on a glass slide, using appropriate spacers to avoid distortion, and imaged them using a Leica SP8 confocal microscope. Image stacks were collected and single images or sets of stacks were obtained to provide detailed information about the progressive development and loss of ear innervation over time. Images were compiled into plates to show the most pertinent details using Corel Draw.

RNA-sequencing

Total RNA was extracted from the whole inner ear of E14.5 embryos. Each individual sample was prepared from both inner ears of the individual embryo, and *Neurod1CKO* and control E14.5 embryos were selected from three litters. The quality of the isolated RNA was analyzed using Bioanalyzer 2100 (Agilent) and a functional test was performed by reverse transcription (RT) and quantitative real-time PCR (qPCR) using oligodT primers for RT and PCR amplification of a 996-bp product of the *Hprt1* gene. The QuantSeq 3'mRNA-Seq Library Prep Kit FWD for Illumina (Lexogen) was used for library preparation from 4 samples per genotype. Next-generation sequencing was performed on an Illumina NextSeq sequencer (NextSeq 500) using a mode enabling the determination of unidirectional 75 bases and indices, following the manufacturer's instructions at the Genomics Core Facility (EMBL Heidelberg, Germany). The number of reads (minimum, 32 million; maximum, 73 million) was filtered out by TrimmomaticPE version 0.36 [23]. Ribosomal RNA and mitochondrial reads were filtered out by Sortmerna [version 2.1b [24]] using default parameters. RNAseq reads were mapped to the mouse genome using STAR [version 2.5.2b [25]] version GRCm38 primary assembly and annotation version M8. A count table was generated by python script htseq-count [version 0.6.1p1, [26]] with the parameter „–m union". The raw RNAseq data were deposited at GEO (http://www.ncbi.nlm.nih.gov/geo/). DESeq2 [v. 1.15.51, [27]] default parameters were used to normalize data and compare the different groups. We selected differentially expressed genes based on an adjusted P-value < 0.1. A 30% change threshold (e.g. Fold change of ≤ 0.3 for down- and ≤ 1.3 for up-regulated) was applied to identify differentially expressed genes between mutant and control inner ears. The enrichment of the functional categories and functional annotation clustering of the differentially expressed genes were performed using DAVID https://david.ncifcrf.gov/ [28] applying a cutoff of Expression Analysis Systematic Explorer (EASE) > 2 and GOTermFinder (https://go.princeton.edu/cgi-bin/GOTermFinder) with a cutoff of 0.01.

Quantitative real-time PCR

Total RNA was isolated from both inner ears of the embryo at E14.5 using TRI Reagent (Sigma-Aldrich T9424). We used 8 embryos for *Neurod1CKO* and 8 embryos for the control group. RNA from both inner ears of one embryo represented one sample. RNA samples (1 μg) were subjected to RT, as described [20]. Following RT, quantitative qPCR was performed with initial activation at 95 °C for 120 s, followed by 40 cycles at 95 °C for 15 s, 60 °C for 30 s, and 72 °C for 30 s using the CFX384™ Real-Time PCR Detection System

(Bio-Rad Laboratories). The primer sequences (pga.mgh.harvard.edu/primerbank/) are listed in Online Resource Table 4. Relative mRNA expression was calculated using the −ΔΔCq method with *Hprt1* as a reference gene. GraphPad Prism software was used for statistical analysis.

Statistical analysis

All comparisons were made between animals with the same genetic background, typically littermates. The number of samples (n) for each comparison are given in the corresponding figures. Phenotyping and data analysis were performed blind to the genotype of the mice. All values are presented either as the mean ± SD or SEM. For statistical analysis, GraphPad Prism software was used. To assess differences, unpaired two-tailed *t*-tests were employed and one-way ANOVA with Dunnett's multiple comparisons test. Significance was determined as $P < 0.05$ (*), $P < 0.01$ (**), $P < 0.001$ (***) or $P < 0.0001$ (****). Complete results of the statistical analyses are included in the figure legends.

Results

Very dense innervation is present in the *Atoh1/Neurod1CKO* cochlea despite the absence of hair cells.

To generate single *Atoh1CKO*, *Neurod1CKO*, and double *Atoh1/Neurod1CKO* mutants, we conditionally ablated $Atoh1^{f/f}$ and $Neurod1^{f/f}$ with $Isl1^{Cre}$ [16]. $Isl1^{Cre}$ is expressed early in the otocyst, effectively recombining in delaminating sensory neurons and in the sensory progenitors of the inner ear ([19,15], Online Resource Fig. 1). No differentiated HCs were detected in any part of the *Atoh1CKO* and *Atoh1/Neurod1CKO* cochlea at P0 compared to littermate controls, as shown by immunolabeling of Myo7a, a hair cell marker (Fig. 1). Most dramatic was the reduction of the density of radial fibers in *Atoh1CKO* compared to controls with fibers doubling back on each other instead of entering the organ of Corti and only a few branches seeming to extend into the area of the undifferentiated organ of Corti (Fig. 1C, D, D'). The densest radial fibers remained in the apex of the *Atoh1CKO* cochlea consistent with previous reports on *Atoh1* deletion mutants [29,13]. This pattern of neuronal degradation follows the *Atoh1* expression gradient from the base to apex of the cochlea [12]. The radial fibers of *Neurod1CKO* were dense and organized similarly to the controls; however, there were noticeable abnormalities [15], e.g. elongated radial fibers, thinner and intertwined fiber bundles, and a missing intraganglionic spiral bundle of efferents (IGSB, Fig. 1E–F'). An additional difference between control and *Neurod1CKO* mice was excessive premature innervation of the organ of Corti, particularly profound in the apex of *Neurod1CKO*, whereas controls show a distinct delay in fiber growth and overall lower fiber density at P0 (Fig. 1B', F', I). In contrast, *Atoh1/Neurod1CKO* innervation was unlike the innervation of *Atoh1CKO, Neurod1CKO* or controls (Fig. 1G–H'). Nerve fibers of double mutants formed a complicated network instead of radial fiber bundles with many knots interlinking fibers going different directions and with thick loops extending beyond the undifferentiated sensory epithelium. Strikingly, very dense innervation was formed in the presumed area of the undifferentiated organ of Corti of double *Atoh1/Neurod1CKO* mutants despite the absence of HCs (in detail Fig. 1H').

The *Neurod1CKO* epithelium is disorganized in the cochlear apex and the cochlea is shorter in *Neurod1CKO* and *Atoh1/Neurod1CKO*.

Although the organ of Corti organization in *Neurod1CKO* was comparable to controls with one row of inner HCs (IHCs) and three rows of outer HCs (OHCs; Fig. 1A–B', E–F'), detailed analyses showed abnormalities in the apical epithelium. The sensory epithelium in the apical tip of *Neurod1CKO* was disorganized with multiple HC rows, disrupted planar cell polarity, and ectopic IHCs among OHCs (Fig. 2A–D). Similar to other *Neurod1* deletion mutants [30,10], the differentiation of HCs (Myo7a$^+$ positive cells) in our *Neurod1CKO* progressed faster throughout the organ of Corti than in controls. At E16.5, differentiated Myo7a$^+$ HCs were detected in the apical end of the developing cochlea of *Neurod1CKO* (arrowhead, Fig. 2F) but not in the apex of littermate controls (Fig. 2E). Additionally, the gradient of differentiation along the medial-lateral axis of the cochlea with IHCs differentiating earlier than OHCs was affected in *Neurod1CKO*. Normally, IHCs differentiate earlier than OHCs [31], as shown in the control cochlea (Fig. 2E, arrow indicates the boundary of differentiated OHC expressing Myo7a in controls). In *Neurod1CKO*, both presumptive OHC and IHC rows extended toward the apex at E16.5 (Fig. 2F). An additional effect associated with *Neurod1* deficiency was the shortening of the cochlea. In *Neurod1CKO* and *Atoh1/Neurod1CKO*, the cochlea was shorter by 22% and by 40%, respectively, compared to the littermate control or to the simple *Atoh1CKO* at E16.5 (Fig. 2G). This morphogenetic effect of the cochlear length reduction indicates a novel genetic interaction of *Atoh1* and *Neurod1*.

The *Atoh1CKO* spiral ganglion initially forms comparably to controls in contrast to the early abnormal formation of the spiral ganglion in both *Neurod1CKO* and double *Atoh1/Neurod1CKO* mutants.

Next, we determined the effects of single and combined *Atoh1* and *Neurod1* deletions on the formation of the spiral ganglion (SG) and its innervation. Before HC differentiation at E14.5, the *Atoh1CKO* auditory ganglion structure (innervation and distribution of neurons) was comparable to control littermates (Fig. 3A, B). In contrast, the formation of the SG of *Neurod1CKO* and *Atoh1/Neurod1CKO* was aberrant already at E14.5 (Fig. 3C, D). Dense disorganized innervation was formed in *Neurod1CKO*, although many fibers were oriented straight towards the sensory epithelium (arrowheads in Fig. 3C). In *Atoh1/Neurod1CKO* compared to *Neurod1CKO*, SG neurons were mostly aggregated into the modiolus with larger patches of neurons missing and neuronal fibers of *Atoh1/Neurod1CKO* did not extend towards the sensory epithelium but instead formed a dense disorganized network with large loops in the E14.5 cochlea (arrows in Fig. 3D).

At P0, noticeably reduced SG with areas of completely missing neurons were found in the *Atoh1CKO* cochlea compared to controls (Fig. 3E, G). Although a large number of SG neurons was still found in the *Atoh1CKO* apex, innervation became extensively reduced in the *Atoh1CKO* compared to controls (Fig. 3F, H). The density of *Neurod1CKO* SG neurons and radial fibers was reduced compared to the control cochlea (Fig. 3E, F, I, J). Note overshooting fibers were found extending directly toward the lateral wall (arrows in Fig. 3I). In contrast, a massive loss of neurons was apparent in *Atoh1/Neurod1CKO* compared to *Atoh1CKO* or *Neurod1CKO* (Fig. 3G–L). Strikingly, considering a substantial reduction of

neurons, immunolabeling for tubulin revealed a dense fiber network in the apex of *Atoh1/Neurod1CKO*, suggesting increased aberrant neuronal fiber growth.

Neuronal fibers grow towards SOX2$^+$ sensory precursors without any differentiated HCs in the organ of Corti of *Atoh1CKO* and *Atoh1/Neurod1CKO*.

To understand how neuronal fibers project towards the sensory epithelium, we evaluated the presence of sensory epithelial cells and innervation (Fig. 4). No Myo7a$^+$ HCs were detected in the *Atoh1CKO* or *Atoh1/Neurod1CKO* organ of Corti (Fig. 4 C, D, G, H). We found initial innervation of the SOX2$^+$ epithelium without any differentiated HCs present in the apex of *Atoh1CKO* and *Atoh1/Neurod1CKO* (arrowheads in Fig. 4D, H). When SOX2$^+$ cells were absent (shown in the base of *Atoh1CKO* and *Atoh1/Neurod1CKO* mutants), the innervation of the presumed organ of Corti was missing (Fig. 4C, G). Massive innervation in the double *Atoh1/Neurod1CKO* is noticeable especially in the apex compared to the control or single *Atoh1CKO* and *Neurod1CKO* mutants (Fig. 4H).

Apoptosis causes a loss of sensory epithelia in both the *Atoh1CKO* and *Atoh1/Neurod1CKO* cochlea.

Our data show that sensory cells and neurons first disappeared from the base of the *Atoh1CKO* and *Atoh1/Neurod1CKO* cochlea, which corresponds to the temporal basal-to-apical differentiation wave of sensory HCs [12]. Whole mount immunostaining of the cochlea at E16.5 showed the missing SOX2$^+$ sensory epithelium from the base with still present SOX2$^+$ cells in the middle part and apex of both *Atoh1CKO* and *Atoh1/Neurod1CKO* compared to controls and *Neurod1CKO* (Fig. 5A–D). Immunostaining for cleaved caspase 3 revealed apoptotic cells among SOX2$^+$ sensory precursors in the middle part of the *Atoh1CKO* and *Atoh1/Neurod1CKO* cochlea (arrowheads in Fig. 5B', D'), whereas no apoptotic cells were detected in controls (Fig. 5A') and *Neurod1CKO* (Fig. 5C'). The SOX2$^+$ sensory epithelium is comparable between the control and mutant apex (Fig. 5A"–D"). In contrast, no detectable increase in caspase 3-positive neurons was found in *Neurod1CKO* to explain the reduction of SG neurons. We analyzed embryos at E11.5, E12.5, and E14.5 and did not identify any noticeable increase in the rate of apoptosis at any analyzed age (data not shown). Previously, we showed that the aberrant migration of inner ear neurons contributes to the abnormalities in the formation of the SG in the developing *Neurod1CKO* [15].

Elimination of *Neurod1* alone or combined with *Atoh1* deletion affects central and peripheral innervation patterns.

Going beyond the obvious differences in cellular organization in the cochlea of the three mutant lines outlined above, we employed tracing with lipophilic dyes to reveal topological details of the innervation and distribution of sensory neurons. Insertion of filter strips with lipophilic dyes with different spectral properties allows visualization of the distribution of sensory neurons and their processes, which can be labeled from a given discrete insertion area. In controls, a distinct segregation of central projections in the cochlear nucleus with labeled fibers from the cochlear base (red) and apex (green) dye applications was evident (Fig. 6A, I). Magenta dye applied to the anterior vestibular end organs (utricle, anterior and horizontal ampullae) labeled the vestibular nerve. Similar injections into the *Atoh1CKO*

mutant ears showed that the central projections of *Atoh1CKO* mice were indistinguishable from those of control littermates, suggesting that the absence of HCs has no influence on the initial central projections and base versus apex fiber segregation in the cochlear nucleus (Fig. 6B). Similarly, vestibular afferents were segregated from cochlear afferents in *Atoh1CKO* (Fig. 6B'). This is consistent with previous reports that the segregation of vestibular and cochlear afferents, and cochlear afferents in the cochlear nucleus is independent of peripheral HC or central target differentiation [32]. In contrast, the central innervation of *Neurod1CKO* showed incomplete segregation with overlapping fibers labeled from the base and apex in the cochlear nucleus (Fig. 6C, C'). These data are consistent with our previous report [15] and demonstrate that *Neurod1* is essential for auditory neuron navigation properties, and central nervous system innervation. Combining conditional deletions of *Atoh1* and *Neurod1* resulted in a loss of the segregation of central axons, as cochlear basal and apical afferents overlapped and formed a widely ramifying and reduced fiber network (Fig. 6D). Note that cochlear afferents were detected in the area of the lateral vestibular nucleus, indicating unsegregated central projections from the inner ear (Fig. 6D'). Strikingly, compared to the substantial loss of SG neurons, the density of fibers in the cochlear nucleus of *Atoh1/Neurod1CKO* appeared more abundant than in the *Neurod1CKO*, similar to the excessive growth of processes into the undifferentiated organ of Corti (Fig. 1H).

The segregated basal and apical cochlear afferents of the auditory nerve were distinguished from the vestibular ganglion in the control and *Atoh1CKO* (Fig. 6E, F). In contrast, the basal and apical cochlear afferents overlapped and intermixed together with vestibular neurons and cochlear neurons (dye-labeled from the cochlear base and apex), forming an aberrant "spiro-vestibular" ganglion in *Neurod1CKO* (Fig. 6G). A similar loss of segregation of central axons and formation of a "spiro-vestibular" ganglion was found in *Atoh1/Neurod1CKO* littermates (Fig. 6H), indicating that the deletion of *Neurod1*, affects axon navigation and ganglion segregation.

Next, we analyzed the spatial segregation of neurons and neuronal fibers in the cochlea. In controls, dye labeling showed spatial segregation in the cochlea between the cochlear base (red) and apex (green). No fibers were labeled from the vestibular dye application in the cochlea of controls (Fig. 7A). In contrast, the same dye applications demonstrated unsegregated and overlapping fibers in the *Atoh1/Neurod1CKO* cochlea (Fig. 7B, in detail 7B'–B"'). Note that neurons and fibers labeled by dye injected into the vestibular end organs were found in the cochlea of *Atoh1/Neurod1CKO* (Fig. 7B"'). Detailed analysis of the middle turn of the *Atoh1/Neurod1CKO* cochlea showed excessive innervation of the area of the presumed organ of Corti with fibers labeled by all three dye applications (Fig. 7B""). Similar disorganization in the cochlea with mingled bundles of fibers and the interlace distribution of neurons interconnecting the apex, base and vestibular end organs was found in *Neurod1CKO* (Fig. 7C–C"'). Together, these results indicate that *Neurod1* deletion is responsible for disorganized and unsegregated innervation within the cochlea without any additional contribution of *Atoh1* elimination.

We next investigated if the excessive fibers in the *Atoh1/Neurod1CKO* mutant are afferents or efferents. We labeled inner ear efferents through targeted applications of dye to the olivocochlear bundle near the midline of the hindbrain and afferents through the application

of dye to the cochlear nucleus. Such applications in controls showed that at E16.5 only some afferents extend to OHCs and project along them toward the base (arrowhead in Fig. 8A, red). In *Atoh1CKO*, there was no detectable afferent nor efferent growth into the region of the organ of Corti (Fig. 8B), consistent with previous reports on full *Atoh1* deletion mice [29] or $Pax2^{Cre};Atoh1^{f/f}$ mice [13]. Note that inner ear efferents formed the intraganglionic spiral bundle on the outer edge of the existing SG and the massive loss of SG neurons in the base of *Atoh1CKO* (arrowheads in Fig. 8B). In the *Atoh1/Neurod1CKO* cochlea, efferent and afferent fibers formed an unusual branching pattern at E16.5 (Fig. 8C). *Neurod1* deletion results in disorganized efferent and afferent innervation in the cochlea of *Neurod1CKO* at E16.5. Compared to controls at E18.5 (Fig. 8E), noticeable changes were found in the *Neurod1CKO* cochlea, including excessive afferent growth to the OHC region, missing intraganglionic spiral bundle, and disorganized radial fibers (Fig. 8F, F'). Combining the loss of *Atoh1* and *Neurod1* resulted in a significant reduction of SG neurons (Fig. 8G) but also excessive growth of processes into the area of the undifferentiated organ of Corti (arrowhead Fig. 8G'). Tracing of a single afferent fiber showed unusual bidirectional projection towards the apex and base in *Atoh1/Neurod1CKO* (Fig. 8G"). It should be noted that in the absence of *Atoh1*, there are no differentiated HCs and therefore, the excessive innervation is neuron autonomous.

Loss of *Neurod1* affected developmental programs of gene expression associated with neuronal development and axon projections.

Our anatomical and molecular analyses indicate that NEUROD1 transcription factor orchestrates axon pathfinding of inner ear neurons, and guidance mechanisms for spatial and functional segregation of auditory and vestibular neurons. Furthermore, the absence of ATOH1 and sensory epithelium does not seem to influence *Neurod1CKO* innervation phenotype. To gain insights into the molecular changes induced by *Neurod1* deletion, we carried out transcriptome analysis (RNAseq) in the E14.5 inner ear, when post-mitotic inner ear neurons are undergoing differentiation and initiate axon projection [33], and HCs start to differentiate [31]. We identified 152 differentially expressed protein coding genes (fold change ≥ 30%; adjusted p value < 0.1) in *Neurod1CKO* compared to controls (n = 4 individual samples/genotype) with 75 up- and 77 down-regulated genes (Fig. 9A, Online Resource Table 1). The gene expression profiles were visualized using hierarchical clustering (Fig. 9B). Gene ontology (GO) terms enrichment analysis of differentially expressed genes revealed that the top GO terms for the biological processes category (enrichment score 8.3) were related to nervous system development and neurogenesis (Fig. 9C, Online Resource Table 2). The full list of enriched GO-terms is provided in Table S3. Consistent with role of NEUROD1 as a neuronal fate driver, the major GO supercluster for down-regulated genes was neuron development, whereas cell adhesion and axonogenesis represented the major GO superclusters for up-regulated genes in the *Neurod1CKO* inner ear. Among enriched GO-terms, neuron projection development, synapse organization, cell migration, cell adhesion, neuron differentiation, and neurogenesis were represented (Online Resource Table 3). For example, down-regulated genes encoding regulatory proteins and transcription factors associated with the promotion of neurogenesis included *Hmga2*, *Bach2*, *Neurod2, Pou4f1*, *Insm1, Nhlh1*, *Nhlh2*, and *Shox2* in the *Neurod1CKO* mutant inner ear. Among genes associated with axon guidance and neurite growth, *Cntn4, Cspg5, Ptn,*

Decorin, Nr2e1, Timp2, Timp3, and *Itga8* were up-regulated, whereas *Ina, Igfbpl1, Igf1, Vegfd*, and *Epha5* were down-regulated. A panel of differentially expressed transcripts from the RNAseq analysis, i.e. *Cntn4, Insm1, Epha5, Shox2, Nhlh1, Hmga2, Isl1, Neurod1, Nr2e1, Pou4f1*, and *Ntrk3*, was validated by qPCR with reverse transcription (RT-qPCR) using additional biological replicates (Fig. 9D). Particularly, decreased expression of *Epha5* and *Pou4f1* correlates with abnormalities in the peripheral and central innervation pattern of SG neurons of *Neurod1CKO*. Eph receptors are involved in axon guidance during early auditory circuit development and EphA5 is enriched in the early SG neurons [34]. Similarly, POU4F1 is important for the early neurogenesis, neuronal migration, and initial axon pathfinding of SG neurons [35]. POU4F1 together with NEUROD1 presumably co-regulate expression of neurotrophin receptors, including tyrosine kinase receptor C (*Ntrk3* [10]), essential for the targeted projections to the brain and the periphery of sensory neurons [9,35]. A loss of *Neurod1* negatively affected the expression of transcriptional regulating factors associated with neurogenesis, such as *Isl1, Insm1, Nhlh1, Shox2*, and *Hmga2*. Among significantly upregulated genes in the *Neurod1CKO* inner ear, we identified the nuclear receptor *Nr2e1* (also known as *Tlx*), essential for maintenance of undifferentiated neural stem cells in adult neurogenesis [36]. Another significantly upregulated gene (a representative of cell adhesion and axonogenesis superclusters) contactin-4 (*Cntn4*) has been shown to promote target-axon specificity [37] and neurite outgrowth and branching [38]. We found that Prox1, which is involved in Type II fiber pathfinding [5], was not detected in SG neurons of *Neurod1CKO* (Fig. 9E, F). Taken together, these analyses provide candidate genes correlating with the *Neurod1* deficiency phenotype of abnormal neuronal development, axon overgrowth, and altered axon pathfinding beyond the apparent expansion of remaining afferents to innervate the epithelium without any HCs in *Atoh1/Neurod1CKO*.

Discussion

In this study, we investigated NEUROD1-ATOH1 interdependency during the development of neurons and sensory cells of the cochlea. Using $Isl1^{Cre}$, we generated new conditional deletions of *Neurod1* and *Atoh1* in the inner ear. We show that significant innervation remodeling (*Neurod1CKO*) or axon retraction and deterioration (*Atoh1CKO*) occur in these mutants. Importantly, we report here for the first time on *Neurod1* and *Atoh1* double conditional mutant mice that display previously unrecognized interactions of ATOH1 and NEUROD1 in inner ear development (summarized in Fig. 10). The double *Atoh1/Neurod1* mutants develop dense afferent innervation of the organ of Corti without any differentiated HCs and extensive central projections to the cochlear nucleus, consistent with an independent effect of either mutation. These data rule out that the *Neurod1* phenotype of disorganized central and premature and excessive peripheral innervation [15] is dependent on *Atoh1*, because we find nearly identical disorganization in *Atoh1/Neurod1CKO* mice.

Elimination of *Atoh1* resulted in apoptosis of sensory precursors and absence of differentiated HCs in the organ of Corti in both our *Atoh1CKO* and *Atoh1/Neurod1CKO* mutants. The absence of HCs and elimination of sensory $SOX2^+$ precursors from the base-to-apex was also reported for other *Atoh1* deletion models [14,13]. We are the first to show nerve fibers reaching sensory $SOX2^+$ precursors in the developing organ of Corti without needing the presence of differentiated HCs (Fig. 4). In all *Atoh1* deficient models including

our single *Atoh1CKO*, only the differentiation of HCs is affected with no effect on morphogenesis or formation of undifferentiated precursors in sensory epithelia. Unexpectedly, we identified a more profound morphogenetic effect of shortening of the cochlea in our double *Atoh1/Neurod1CKO*. The *Atoh1/Neurod1CKO* cochlea is even more truncated compared to *Neurod1CKO*, indicating additional unrecognized genetic interactions between these bHLH factors (Fig. 2G). Previous work suggested that truncated growth in the cochlea of *Neurod1* null mice is a result of alternations in spatiotemporal gene expression [10]. A similar extent of cochlear truncation was shown in a *Neurog1* null mutant [8]. How these bHLH factors are interconnected in a gene regulatory network effecting cochlear morphogenesis remains unclear.

The neuronal phenotypes of our *Neurod1CKO* and double *Atoh1/Neurod1CKO* mutants show a number of novel features. In both these mutants, some SG neurons were translocated and formed, together with vestibular ganglion neurons, an aberrant “spiro-vestibular” ganglion, described previously in *Neurod1CKO* [15]. Accordingly, the central axons were not segregated in the auditory and vestibular nerve but overlapping fibers formed an aberrant auditory-vestibular nerve. Our dye tracing experiments showed some neurons of the SG were connected with HCs in the cochlear base and apex, and some neurons residing in the SG had connections to vestibular organs in both *Neurod1CKO* and *Atoh1/Neurod1CKO*. Thus, the peripheral processes extending towards the organ of Corti, central projections, and migration properties of inner ear sensory neurons are affected by the deletion of *Neurod1* without any additional influence of ATOH1.

Previous studies generated *Atoh1* and *Neurod1* deletions in both the ear and the central auditory nuclei, significantly affecting the development of the cochlear nucleus and limiting assessment of the wiring defects [30,29,13]. In contrast, *Isl1-Cre* is not expressed in the cochlear nucleus and inferior colliculus [15], and therefore, our mutants retain *Atoh1* and *Neurod1* expression in the auditory nuclei and auditory midbrain. We extended previous suggestions that segregation of vestibular and cochlear afferents within the hindbrain is not affected by *Atoh1* deletion [32]. For the first time, we show that the central projections of the cochlear nucleus and the tonotopic organization of the cochlear nucleus subdivisions in *Atoh1CKO* was virtually indistinguishable from the control, suggesting normal central axon pathfinding of inner ear neurons without any differentiated sensory epithelium. Thus, a subsequent loss of central axons is exclusively a secondary effect of neuronal death accompanying apoptosis of the sensory epithelium in the *Atoh1CKO* inner ear. In contrast, the tonotopic segregation was lost and overall coverage of the cochlear nucleus was considerably reduced in our *Neurod1CKO* and *Atoh1/Neurod1CKO* mutants compared to the control and *Atoh1CKO*. Our data suggest that NEUROD1 regulates the correct wiring of SG neurons to the cochlear nucleus independently of ATOH1, as evidenced by the same disorganization of central axons in the *Neurod1CKO* [15] and *Atoh1/Neurod1CKO* cochlear nucleus.

We also showed that combining the loss of *Atoh1* with loss of *Neurod1* resulted in an unusual pattern of premature fiber extension to the organ of Corti in the absence of any differentiated HCs or supporting cells, i.e. flat epithelia. Innervation of such flat epithelia can be driven by neurotrophin expression through residual supporting cell differentiation

[13] or viral transfection [39]. However, no excessive innervation was detected in our simple *Atoh1CKO* mice, thus ruling out any partial supporting cell differentiation. Therefore, the outgrowth of afferents detected in the *Neurod1CKO* apex is not driven by premature HC differentiation and/or their transformation but is SG neuron autonomous. By logical extension, we also show for the first time that the outgrowth of extending peripheral axons in simple *Neurod1CKO* mutant mice is not regulated by unregulated expression of ATOH1 in neurons, as the overall pattern of growth is similar to the double *Atoh1/Neurod1CKO*.

Our anatomical and molecular analyses indicate that NEUROD1 transcription factor orchestrates neurite growth, axon pathfinding of inner ear neurons, neuronal migration and guidance mechanisms for spatial and functional segregation of auditory and vestibular neurons. A number of genes affected in our *Neurod1CKO* have been implicated in determining SG ganglion size and abnormal innervation. For example, reduced *Pou4f1* (also known as *Brn3a*) [40] and *Ntrk3* (also known as *TrkC*) [41] are associated with the topographical losses of sensory neurons and misrouting axon projections in the basal turn of the cochlea. The more severe phenotype of our *Neurod1CKO* in axon projections and neuronal loss is in line with prior suggestions of NEUROD1 acting upstream of POU4F1 in a hierarchical transcriptional network controlling inner ear sensory neuron development [42]. Another member of the cascade of transcription factors regulating the development of inner ear neurons negatively affected by *Neurod1* deletion is INSM1. *Insm1*$^{-/-}$ inner ear have a reduced number of vestibular and auditory neurons due to reduced proliferation of delaminated neuronal progenitors [43]. Similar to our *Neurod1CKO*, no significant increase in apoptosis was found in the inner ear ganglia of *Insm1*$^{-/-}$. Interestingly, in the absence of *Insm1* some OHCs transdifferentiate into IHCs [44] similar to the sensory phenotype found in the apex of our *Neurod1CKO* and other *Neurod1* deletion mutants [10,30]. This indicates a possible interaction of NEUROD1 and INSM1 in nascent HCs in the apex. Reduced expression of *Epha5* correlates with axon guidance and neuronal migration defects of *Neurod1CKO* [45].

Further experiments will be needed to fully identify the guidance mechanisms that may be altered by *Neurod1* mutation specifically in auditory neurons and to determine whether the observed increased innervation following *Neurod1* knockout has any potential therapeutic benefits in models of hearing loss. This includes enhancing understanding of how innervation can be stabilized in the long term after age-related loss of HCs [46], ototoxic drug [47] or sound induced hearing loss, including neuropathy [48] and for more effective nerve growth to support a cochlear implant [49].

Supplementary Material

Refer to Web version on PubMed Central for supplementary material.

Funding

This study was supported by a grant from the Czech Science Foundation (20-06927S to GP); by BIOCEVCZ.1.05/1.1.00/02.0109 from the ERDF; by the institutional support of the Czech Academy of Sciences RVO: 86652036; and by NIH (R01 AG060504 to BF). We thank O. Benada of the Electron Microscopy Group (Institute of Microbiology CAS) for assistance with SEM and acknowledge the support of the Imaging Methods

Core Facility at BIOCEV funded by the Czech-BioImaging large RI projects (LM2015062 and CZ.02.1.01/0.0/0.0/16_013/0001775, from MEYS CR).

REFERENCES

1. Driver EC, Kelley MW (2020) Development of the cochlea. Development 147 (12). doi:10.1242/dev.162263
2. Zou D, Silvius D, Fritzsch B, Xu P-X (2004) Eya1 and Six1 are essential for early steps of sensory neurogenesis in mammalian cranial placodes. Development 131 (22):5561–5572 [PubMed: 15496442]
3. Kiernan AE, Pelling AL, Leung KK, Tang AS, Bell DM, Tease C, Lovell-Badge R, Steel KP, Cheah KS (2005) Sox2 is required for sensory organ development in the mammalian inner ear. Nature 434 (7036):1031–1035 [PubMed: 15846349]
4. Karis A, Pata I, van Doorninck JH, Grosveld F, de Zeeuw CI, de Caprona D, Fritzsch B (2001) Transcription factor GATA-3 alters pathway selection of olivocochlear neurons and affects morphogenesis of the ear. J Comp Neurol 429 (4):615–630 [PubMed: 11135239]
5. Bouchard M, de Caprona D, Busslinger M, Xu P, Fritzsch B (2010) Pax2 and Pax8 cooperate in mouse inner ear morphogenesis and innervation. BMC developmental biology 10 (1):89 [PubMed: 20727173]
6. Raft S, Groves AK (2014) Segregating neural and mechanosensory fates in the developing ear: patterning, signaling, and transcriptional control. Cell and tissue research. doi:10.1007/s00441-014-1917-6
7. Fritzsch B, Elliott KL (2017) Gene, cell, and organ multiplication drives inner ear evolution. Developmental Biology 431 (1):3–15. doi:10.1016/j.ydbio.2017.08.034 [PubMed: 28866362]
8. Ma Q, Anderson DJ, Fritzsch B (2000) Neurogenin 1 null mutant ears develop fewer, morphologically normal hair cells in smaller sensory epithelia devoid of innervation. Journal of the Association for Research in Otolaryngology 1 (2):129–143 [PubMed: 11545141]
9. Kim W-Y, Fritzsch B, Serls A, Bakel LA, Huang EJ, Reichardt LF, Barth DS, Lee JE (2001) NeuroD-null mice are deaf due to a severe loss of the inner ear sensory neurons during development. Development 128 (3):417–426 [PubMed: 11152640]
10. Jahan I, Pan N, Kersigo J, Fritzsch B (2010) Neurod1 suppresses hair cell differentiation in ear ganglia and regulates hair cell subtype development in the cochlea. PloS one 5 (7):e11661. doi:10.1371/journal.pone.0011661 [PubMed: 20661473]
11. Kopecky BJ, Jahan I, Fritzsch B (2013) Correct timing of proliferation and differentiation is necessary for normal inner ear development and auditory hair cell viability. Developmental Dynamics 242 (2):132–147 [PubMed: 23193000]
12. Pan N, Jahan I, Kersigo J, Duncan JS, Kopecky B, Fritzsch B (2012) A novel Atoh1 “self-terminating” mouse model reveals the necessity of proper Atoh1 level and duration for hair cell differentiation and viability. PloS one 7 (1):e30358. doi:10.1371/journal.pone.0030358 [PubMed: 22279587]
13. Pan N, Jahan I, Kersigo J, Kopecky B, Santi P, Johnson S, Schmitz H, Fritzsch B (2011) Conditional deletion of Atoh1 using Pax2-Cre results in viable mice without differentiated cochlear hair cells that have lost most of the organ of Corti. Hearing research 275 (1–2):66–80. doi:10.1016/j.heares.2010.12.002 [PubMed: 21146598]
14. Bermingham N, Hassan B, Price S, Vollrath M, Ben-Arie N, Eatock R, Bellen H, Lysakowski A, Zoghbi H (1999) Math1: an essential gene for the generation of inner ear hair cells. Science (284):1837–1841
15. Macova I, Pysanenko K, Chumak T, Dvorakova M, Bohuslavova R, Syka J, Fritzsch B, Pavlinkova G (2019) Neurod1 Is Essential for the Primary Tonotopic Organization and Related Auditory Information Processing in the Midbrain. J Neurosci 39 (6):984–1004. doi:10.1523/JNEUROSCI.2557-18.2018 [PubMed: 30541910]
16. Yang L, Cai CL, Lin L, Qyang Y, Chung C, Monteiro RM, Mummery CL, Fishman GI, Cogen A, Evans S (2006) Isl1Cre reveals a common Bmp pathway in heart and limb development. Development 133 (8):1575–1585. doi:10.1242/dev.02322 [PubMed: 16556916]

17. Goebbels S, Bode U, Pieper A, Funfschilling U, Schwab MH, Nave KA (2005) Cre/loxP-mediated inactivation of the bHLH transcription factor gene NeuroD/BETA2. Genesis 42 (4):247–252. doi:10.1002/gene.20138 [PubMed: 16028233]

18. Shroyer NF, Helmrath MA, Wang VY, Antalffy B, Henning SJ, Zoghbi HY (2007) Intestine-specific ablation of mouse atonal homolog 1 (Math1) reveals a role in cellular homeostasis. Gastroenterology 132 (7):2478–2488. doi:10.1053/j.gastro.2007.03.047 [PubMed: 17570220]

19. Dvorakova M, Jahan I, Macova I, Chumak T, Bohuslavova R, Syka J, Fritzsch B, Pavlinkova G (2016) Incomplete and delayed Sox2 deletion defines residual ear neurosensory development and maintenance. Sci Rep 6:38253. doi:10.1038/srep38253 [PubMed: 27917898]

20. Bohuslavova R, Dodd N, Macova I, Chumak T, Horak M, Syka J, Fritzsch B, Pavlinkova G (2017) Pax2-Islet1 Transgenic Mice Are Hyperactive and Have Altered Cerebellar Foliation. Mol Neurobiol 54 (2):1352–1368. doi:10.1007/s12035-016-9716-6 [PubMed: 26843111]

21. Fritzsch B, Duncan JS, Kersigo J, Gray B, Elliott KL (2016) Neuroanatomical Tracing Techniques in the Ear: History, State of the Art, and Future Developments In: Sokolowski B, Ed: Auditory and Vestibular Research: Methods and Protocols, vol 1427 Springer Science+Business Media New York, pp 243–262

22. Simmons D, Duncan J, de Caprona DC, Fritzsch B (2011) Development of the inner ear efferent system In: Auditory and vestibular efferents. Springer, pp 187–216

23. Bolger AM, Lohse M, Usadel B (2014) Trimmomatic: a flexible trimmer for Illumina sequence data. Bioinformatics 30 (15):2114–2120. doi:10.1093/bioinformatics/btu170 [PubMed: 24695404]

24. Kopylova E, Noe L, Touzet H (2012) SortMeRNA: fast and accurate filtering of ribosomal RNAs in metatranscriptomic data. Bioinformatics 28 (24):3211–3217. doi:10.1093/bioinformatics/bts611 [PubMed: 23071270]

25. Dobin A, Davis CA, Schlesinger F, Drenkow J, Zaleski C, Jha S, Batut P, Chaisson M, Gingeras TR (2013) STAR: ultrafast universal RNA-seq aligner. Bioinformatics 29 (1):15–21. doi:10.1093/bioinformatics/bts635 [PubMed: 23104886]

26. Anders S, Pyl PT, Huber W (2015) HTSeq--a Python framework to work with high-throughput sequencing data. Bioinformatics 31 (2):166–169. doi:10.1093/bioinformatics/btu638 [PubMed: 25260700]

27. Love MI, Huber W, Anders S (2014) Moderated estimation of fold change and dispersion for RNA-seq data with DESeq2. Genome Biol 15 (12):550. doi:10.1186/s13059-014-0550-8 [PubMed: 25516281]

28. Huang da W, Sherman BT, Lempicki RA (2009) Systematic and integrative analysis of large gene lists using DAVID bioinformatics resources. Nat Protoc 4 (1):44–57. doi:10.1038/nprot.2008.211 [PubMed: 19131956]

29. Fritzsch B, Matei VA, Nichols DH, Bermingham N, Jones K, Beisel KW, Wang VY (2005) Atoh1 null mice show directed afferent fiber growth to undifferentiated ear sensory epithelia followed by incomplete fiber retention. Dev Dyn 233 (2):570–583 [PubMed: 15844198]

30. Liu M, Pereira FA, Price SD, Chu M-j, Shope C, Himes D, Eatock RA, Brownell WE, Lysakowski A, Tsai M-J (2000) Essential role of BETA2/NeuroD1 in development of the vestibular and auditory systems. Genes & development 14 (22):2839–2854 [PubMed: 11090132]

31. Tateya T, Sakamoto S, Ishidate F, Hirashima T, Imayoshi I, Kageyama R (2019) Three-dimensional live imaging of Atoh1 reveals the dynamics of hair cell induction and organization in the developing cochlea. Development 146 (21). doi:10.1242/dev.177881

32. Elliott KL, Kersigo J, Pan N, Jahan I, Fritzsch B (2017) Spiral ganglion neuron projection development to the hindbrain in mice lacking peripheral and/or central target differentiation. Frontiers in neural circuits 11:25 [PubMed: 28450830]

33. Yang T, Kersigo J, Jahan I, Pan N, Fritzsch B (2011) The molecular basis of making spiral ganglion neurons and connecting them to hair cells of the organ of Corti. Hearing research 278 (1–2):21–33 [PubMed: 21414397]

34. Lu CC, Appler JM, Houseman EA, Goodrich LV (2011) Developmental profiling of spiral ganglion neurons reveals insights into auditory circuit assembly. J Neurosci 31 (30):10903–10918. doi:10.1523/JNEUROSCI.2358-11.2011 [PubMed: 21795542]

35. Fariñas I, Jones KR, Tessarollo L, Vigers AJ, Huang E, Kirstein M, De Caprona DC, Coppola V, Backus C, Reichardt LF (2001) Spatial shaping of cochlear innervation by temporally regulated neurotrophin expression. Journal of Neuroscience 21 (16):6170–6180 [PubMed: 11487640]
36. Shi Y, Chichung Lie D, Taupin P, Nakashima K, Ray J, Yu RT, Gage FH, Evans RM (2004) Expression and function of orphan nuclear receptor TLX in adult neural stem cells. Nature 427 (6969):78–83. doi:10.1038/nature02211 [PubMed: 14702088]
37. Osterhout JA, Stafford BK, Nguyen PL, Yoshihara Y, Huberman AD (2015) Contactin-4 mediates axon-target specificity and functional development of the accessory optic system. Neuron 86 (4):985–999. doi:10.1016/j.neuron.2015.04.005 [PubMed: 25959733]
38. Mercati O, Danckaert A, Andre-Leroux G, Bellinzoni M, Gouder L, Watanabe K, Shimoda Y, Grailhe R, De Chaumont F, Bourgeron T, Cloez-Tayarani I (2013) Contactin 4, −5 and −6 differentially regulate neuritogenesis while they display identical PTPRG binding sites. Biol Open 2 (3):324–334. doi:10.1242/bio.20133343 [PubMed: 23519440]
39. Shibata SB, Budenz CL, Bowling SA, Pfingst BE, Raphael Y (2011) Nerve maintenance and regeneration in the damaged cochlea. Hearing research 281 (1–2):56–64. doi:10.1016/j.heares.2011.04.019 [PubMed: 21596129]
40. Huang EJ, Liu W, Fritzsch B, Bianchi LM, Reichardt LF, Xiang M (2001) Brn3a is a transcriptional regulator of soma size, target field innervation and axon pathfinding of inner ear sensory neurons. Development 128 (13):2421–2432 [PubMed: 11493560]
41. Fritzsch B, Barbacid M, Silos-Santiago I (1998) The combined effects of trkB and trkC mutations on the innervation of the inner ear. Int J Dev Neurosci 16 (6):493–505 [PubMed: 9881298]
42. Deng M, Yang H, Xie X, Liang G, Gan L (2014) Comparative expression analysis of POU4F1, POU4F2 and ISL1 in developing mouse cochleovestibular ganglion neurons. Gene Expr Patterns 15 (1):31–37. doi:10.1016/j.gep.2014.03.001 [PubMed: 24709358]
43. Lorenzen SM, Duggan A, Osipovich AB, Magnuson MA, Garcia-Anoveros J (2015) Insm1 promotes neurogenic proliferation in delaminated otic progenitors. Mech Dev 138 Pt 3:233–245. doi:10.1016/j.mod.2015.11.001 [PubMed: 26545349]
44. Wiwatpanit T, Lorenzen SM, Cantú JA, Foo CZ, Hogan AK, Márquez F, Clancy JC, Schipma MJ, Cheatham MA, Duggan A (2018) Trans-differentiation of outer hair cells into inner hair cells in the absence of INSM1. Nature:1
45. Cramer KS (2005) Eph proteins and the assembly of auditory circuits. Hearing research 206 (1–2):42–51. doi:10.1016/j.heares.2004.11.024 [PubMed: 16080997]
46. Frisina RD, Ding B, Zhu X, Walton JP (2016) Age-related hearing loss: prevention of threshold declines, cell loss and apoptosis in spiral ganglion neurons. Aging (Albany NY) 8 (9):2081 [PubMed: 27667674]
47. Sha S-H, Schacht J (2017) Emerging therapeutic interventions against noise-induced hearing loss. Expert opinion on investigational drugs 26 (1):85–96 [PubMed: 27918210]
48. Fernandez KA, Jeffers PW, Lall K, Liberman MC, Kujawa SG (2015) Aging after noise exposure: acceleration of cochlear synaptopathy in “recovered” ears. J Neurosci 35 (19):7509–7520. doi:10.1523/JNEUROSCI.5138-14.2015 [PubMed: 25972177]
49. Abbas PJ, Tejani VD, Scheperle RA, Brown CJ (2017) Using neural response telemetry to monitor physiological responses to acoustic stimulation in hybrid cochlear implant users. Ear and hearing 38 (4):409–425 [PubMed: 28085738]

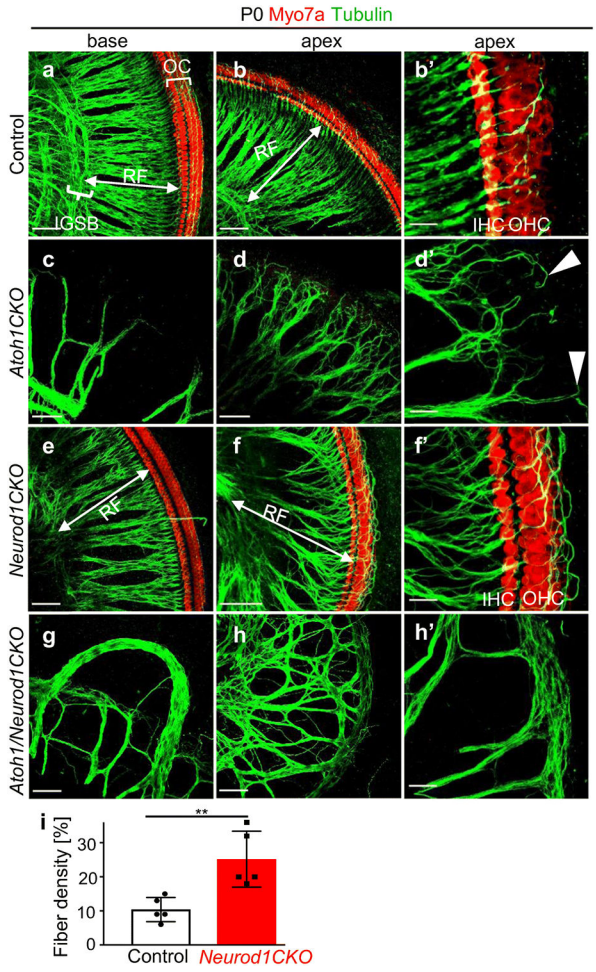

Figure 1. The combined deletion of *Atoh1* and *Neurod1* results in a loss of the sensory hair cells and unusual interlaced innervation in the cochlea.

(**A-H**) Compared to the four rows of hair cells (HCs, labeled by Myo7a, a marker of HCs) in the control and *Neurod1CKO* cochlear base and apex, deletion of *Atoh1* results in a complete loss of HCs in both *Atoh1CKO* and *Atoh1/Neurod1CKO* mutants, shown in whole mount immunostaining of the cochlea. As a consequence, neuronal fibers (labeled by tubulin) are affected in both these *CKO* mutants but in the double mutant, fibers form complicated network with loops and knots. Radial fibers of *Neurod1CKO* are less dense and longer, and the intraganglionic spiral bundle (IGSB) is not formed compared to the controls. (**A'-H'**) Higher-magnification images show the control littermate with many neuronal axons still not reaching their target outer HCs in the apex at P0. In contrast, the nerve fibers of *Neurod1CKO* reach the lateral part of the organ of Corti and form a dense disorganized axon net over the sensory epithelium. In *Atoh1CKO*, the loss of the sensory epithelium results in the retraction and doubling back of nerve fibers (arrowheads in D'), whereas the double deletion of *Atoh1* and *Neurod1* leads to the formation of abnormal long axons and dense network of fibers in the area of the presumed organ of Corti of *Atoh1/Neurod1CKO* (H'). (**I**) Quantification of fiber density in the area of the organ of Corti of *Neurod1CKO* (n = 5) and controls (n = 5). The values represent mean ± SD, *t*-test, **P < 0.01. IHC, inner hair cells;

OC, organ of Corti; OHC, outer hair cells; RF, radial fibers. Scale bars: 50 μm (A-H); 20 μm (B', D', F', H').

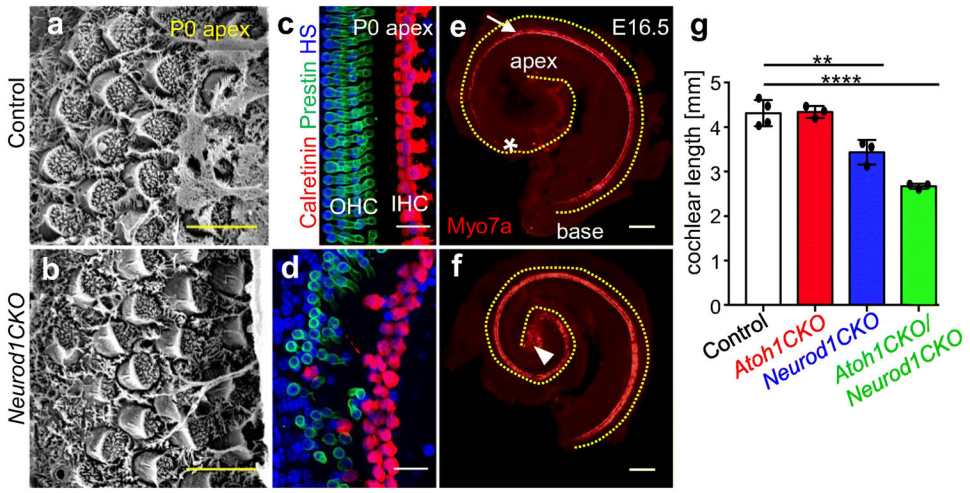

Figure 2. Sensory epithelium is disorganized in the apex of *Neurod1CKO* and the length of the organ of Corti is reduced in *Neurod1CKO* and *Atoh1/Neurod1CKO*.

(**A-D**) In contrast to controls, the sensory epithelium in the apex of *Neurod1CKO* contains multiple hair cell rows and disrupted planar cell polarity (A, B scanning electron microscopy), and ectopic inner HCs (IHC) among outer HCs (OHC), as shown by confocal images of immunolabeling with IHC marker calretinin (red) and prestin, marker of OHC (green). (**E, F**) Whole mount immunolabeled cochlea shows differentiated Myo7a^{+} HCs (red) in the apex of *Neurod1CKO* (arrowhead) but not in the control apex. Asterisk indicates the border of the latest differentiated Myo7a^{+} HCs. Note the missing gradient of differentiation along the medial-lateral axis of the organ of Corti of *Neurod1CKO* with both IHCs and OHCs simultaneously differentiated in the apex at E16.5. In controls, IHCs are differentiating earlier than OHCs (arrow indicates the boundary of differentiated Myo7a^{+} OHCs). The cochlea is delineated by yellow dotted line. (**G**) The cochlear length in the area corresponding to the organ of Corti of *Neurod1CKO* and *Atoh1/Neurod1CKO* is 22% and 40% shorter than controls, respectively. The values represent mean ± SD (n = 4 for controls, n = 3 for mutants), Dunnett's multiple comparisons test, one-way ANOVA **P < 0.01, ****P < 0.0001. Scale bars: 5 μm (A, B); 20 μm (C, D); 200 μm (E, F); HS, Hoechst nuclear staining.

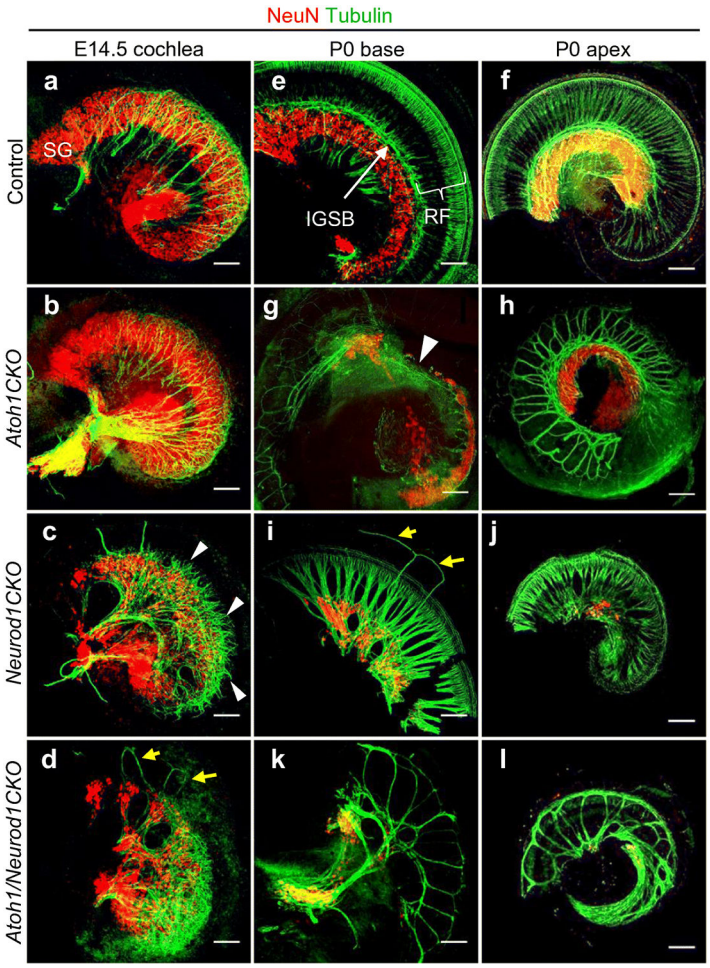

Figure 3. *Atoh1* deletion in the sensory epithelium affects the survival of neurons, whereas a loss of *Neurod1* alters the formation of the spiral ganglion.

(**A-D**) Whole mount immunolabeling of the cochlea with anti-NeuN (nuclear marker of differentiated neurons) and with anti-tubulin shows the comparable formation and size of spiral ganglion (SG) between control and *Atoh1CKO* at E14.5. In contrast, deletion of *Neurod1* in *Neurod1CKO* and in *Atoh1/Neurod1CKO* results in a phenotype with an altered formation of the SG at E14.5. Note fibers in *Neurod1CKO* are oriented straight towards the sensory epithelium (arrowheads) and the overshooting fiber loops in *Atoh1/Neurod1CKO* (arrows in D). (**E-H**) At P0, *Atoh1CKO* SG neurons are missing in the base (arrowhead) and still present in the apex; however, the deterioration of innervation is noticeable along the whole cochlea compared to control littermates. (**I, J**) The overall density of *Neurod1CKO* SG neurons and radial fibers (RF) is lower with a missing intraganglionic spiral bundle (IGSB) compared to the control at P0. Overshooting fibers are detected in the cochlea of *Neurod1CKO* (arrows in I). The apex of *Neurod1CKO* is innervated but the number of neurons is severely reduced. (**K, L**) The SG of *Atoh1/Neurod1CKO* is severely reduced with a few patches of neurons detected in the area corresponding to the SG, and altered innervation with unusual thick fibers, especially in the apex. Scale bars: 100 μm.

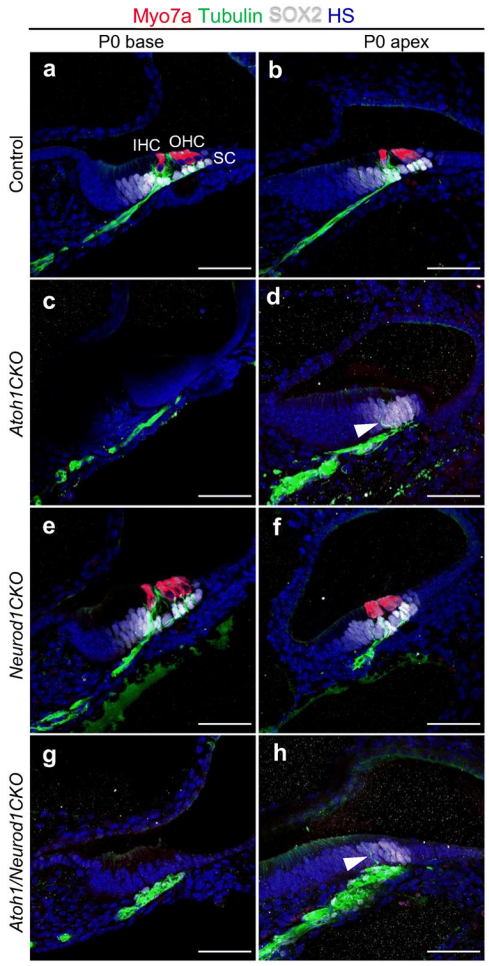

Figure 4. Neuronal fibers in the *Atoh1CKO* and *Atoh1/Neurod1CKO* cochlea innervate SOX2 positive sensory epithelium without any differentiated hair cells.

Immunohistochemistry for Myo7a (marker for hair cells, HCs), SOX2 (marker of sensory precursors and supporting cells), and tubulin (nerve fibers) in the vibratome sections of the cochlea shows nerve fibers innervating the sensory epithelium with $Myo7a^+$ HCs and $SOX2^+$ supporting cells in the control (**A**, **B**) and *Neurod1CKO* cochlea (**E**, **F**). (**C**, **G**) The base of *Atoh1CKO* and *Atoh1/Neurod1CKO* does not contain any $Myo7a^+$ and $SOX2^+$ sensory epithelium. (**D**, **H**) Neuronal fibers (arrowhead) project into the $SOX2^+$ epithelium with missing $Myo7a^+$ HCs in the apex of *Atoh1CKO* and *Atoh1/Neurod1CKO*. Note the excessive innervation in the apex of *Atoh1/Neurod1CKO*. Scale bars: 50 μm. HS, Hoechst nuclear staining; IHC, inner hair cells; OHC, outer hair cells; SC, supporting cells.

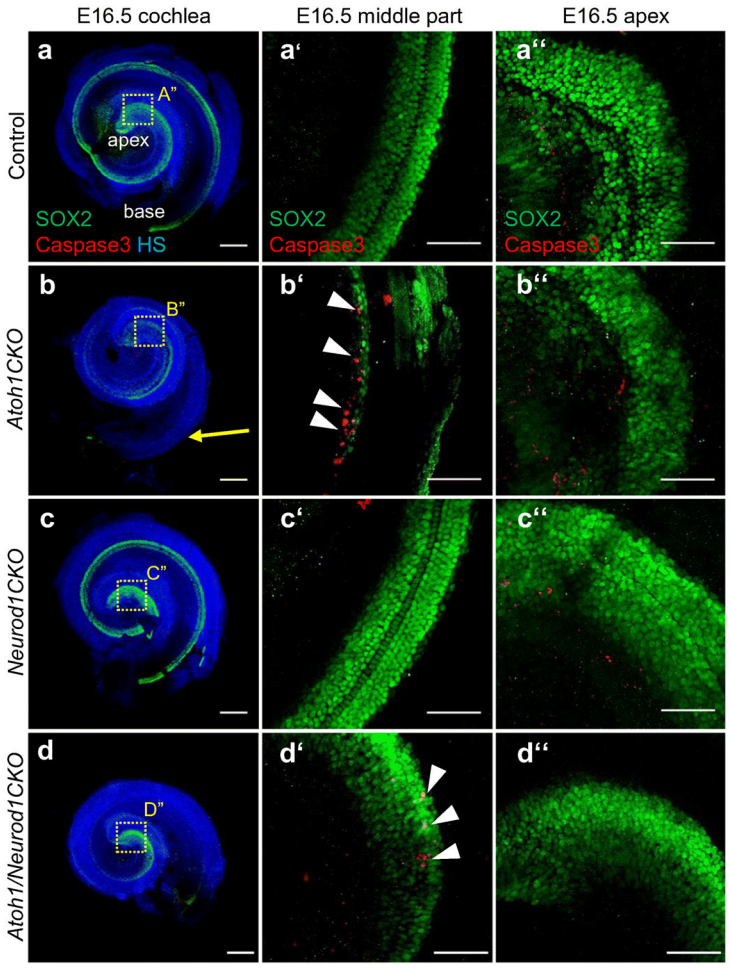

Figure 5. Sensory epithelium precursors in *Atoh1CKO* and *Atoh1/Neurod1CKO* cochlea die by apoptosis.

(**A-A”**) Whole mount immunostaining of the control cochlea with anti-SOX2 and anti-cleaved caspase 3 shows sensory epithelium without any detectable apoptotic cells at E16.5. (**B-B”**) In the *Atoh1CKO* midbase, the majority of $SOX2^+$ epithelial cells are missing (arrow in B) and apoptotic $Caspase\text{-}3^+$ cells are detected (red, arrowheads in B’). (**C-C”**) No apoptotic cells are found in the sensory epithelium of *Neurod1CKO*. (**D-D”**) $SOX2^+$ domain is reduced in the *Atoh1/Neurod1CKO* cochlea as in *Atoh1CKO* with the majority of $SOX2^+$ cells missing in the midbase and with the apex seemingly unaffected. Scale bars: 200 μm (A-D); 50 μm (A’-D”). HS, Hoechst nuclear staining.

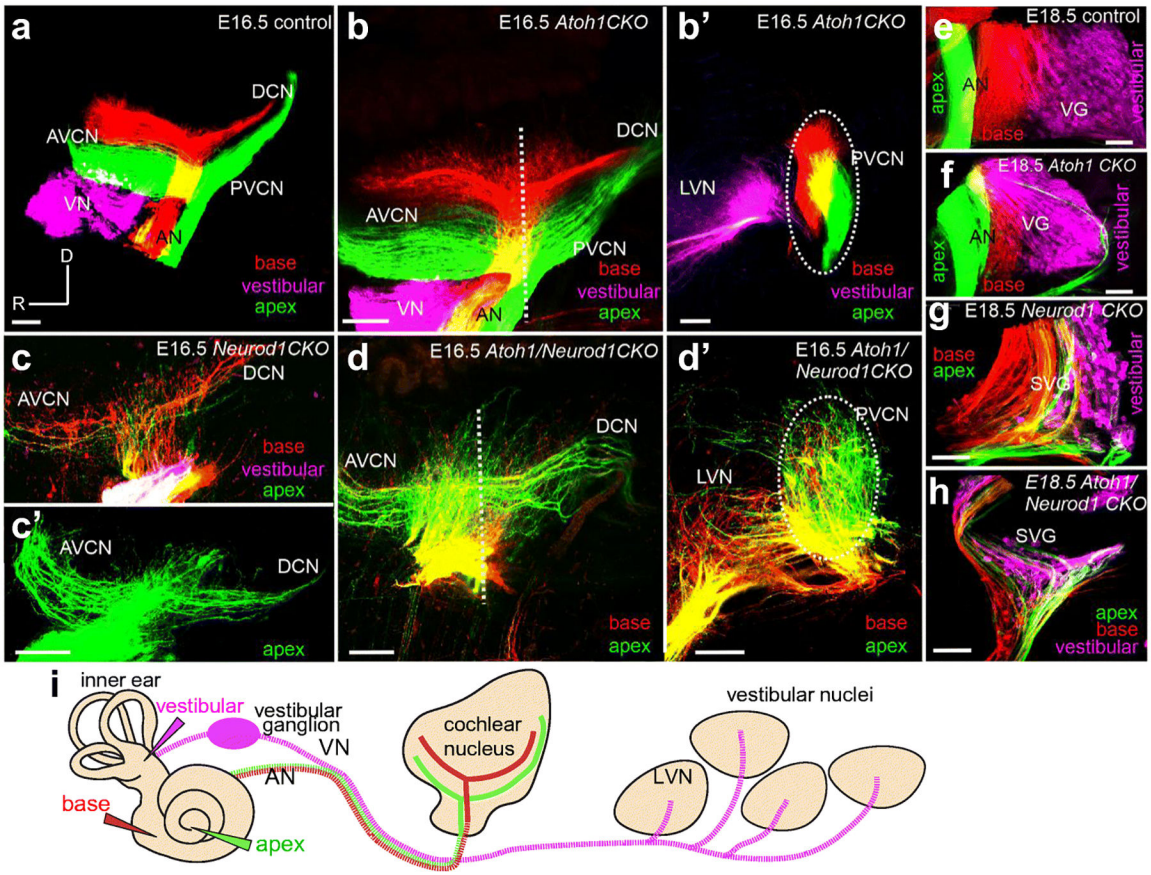

Figure 6. Dye tracing revealed aberrant central projections from the inner ear of *Neurod1CKO* and *Atoh1/Neurod1CKO*.

(**A**) Dye-labeling shows two segregated bands of central projections to the brainstem cochlear nucleus (CN) complex [the anterior ventral CN (AVCN), posterior ventral CN (PVCN), and dorsal CN (DCN)], and the distinct vestibular nerve in the control. Dorsal (D) is up and rostral (R) is to the left. (**B**) A similar organization of the CN subdivisions is in *Atoh1CKO*. The plane of section of the PVCN is indicated by the dotted line. (**B'**) The section of the PVCN shows segregation of cochlear afferents in dorsal and ventral parts of the PVCN (dotted oval), and the segregation of vestibular afferents to the lateral vestibular nucleus (LVN, labeled by dye inserted into the vestibular organs) in *Atoh1CKO*. (**C**) Deletion of *Neurod1* results in unsegregated and overlapping central projections from the cochlea and vestibular organs in *Neurod1CKO*. (**C'**) Single color image shows disorganized fibers in the CN labeled by dye injected in the apex of *Neurod1CKO*. (**D**) Combined deletion of *Atoh1* and *Neurod1* results in the *Neurod1CKO*-like overlapping cochlear projections. The section (**D'**) shows the near complete overlap of afferents from the cochlear base and apex to the PVCN (dotted oval) and cochlear fibers innervating the LVN in *Atoh1/Neurod1CKO*. (**EH**) Segregated central axons from the apex and base form the auditory nerve that is separated from the vestibular ganglion (VG) in controls (E) and in *Atoh1CKO* mutants (F). In contrast, central cochlear and vestibular axons are not segregated and neurons labeled by vestibular, apical, and basal dye applications form an aberrant "spiro-vestibular" ganglion (SVG) in the inner ear of *Neurod1CKO* (G) and *Atoh1/Neurod1CKO*

(H). (**I**) Schematic diagram of dye tracing from the inner ear using insertions of differently colored dyes into the vestibular organs (magenta), cochlear base (red), and apex (green). Scale bars: 100 μm. AN, auditory nerve; SVG, “spiro-vestibular” ganglion; VN, vestibular nerve.

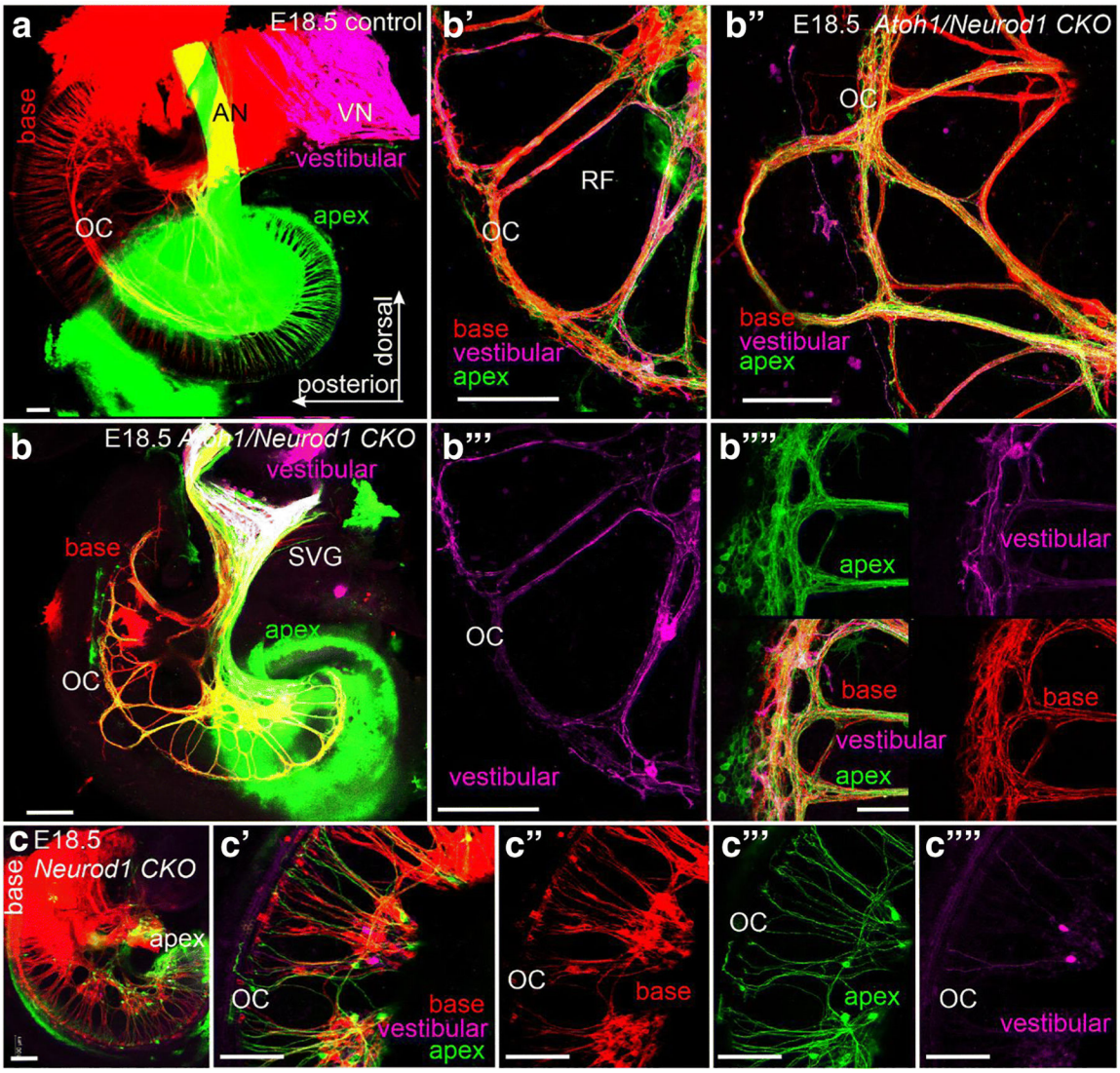

Figure 7. Distribution of multiple and interconnected innervation from the auditory and vestibular systems unveils disorganization in the inner ear of *Atoh1/Neurod1CKO*.

(**A**) Dye applications to the vestibular end organs (magenta), cochlear apex (green) and base (red) show spatially restricted labeling based on the injection site in controls. (**B**) Similar dye applications in double *Atoh1/Neurod1CKO* demonstrate overlapping and unsegregated pattern of innervation in the mutant cochlea. (**B'-B"'**) Detailed analysis of the middle turn of the *Atoh1/Neurod1CKO* cochlea shows fibers and neurons labeled by the vestibular dye application mingled with fibers labeled by dyes applied to the cochlear base and apex. (**B""**) Images of individual colors of the separate channels and a merged image indicate dense, disorganized, and unsegregated innervation in the area of the organ of Corti of *Atoh1/Neurod1CKO*. (**C-C""**) The interlace distribution of fibers and neurons interconnecting the base, apex and vestibular end organs demonstrate the disorganized organization of the *Neurod1CKO* cochlea. Scale bars: 100 μm. AN, auditory nerve; OC, the organ of Corti; RF, radial fibers; SVG, "spiro-vestibular" ganglion; VN, vestibular nerve.

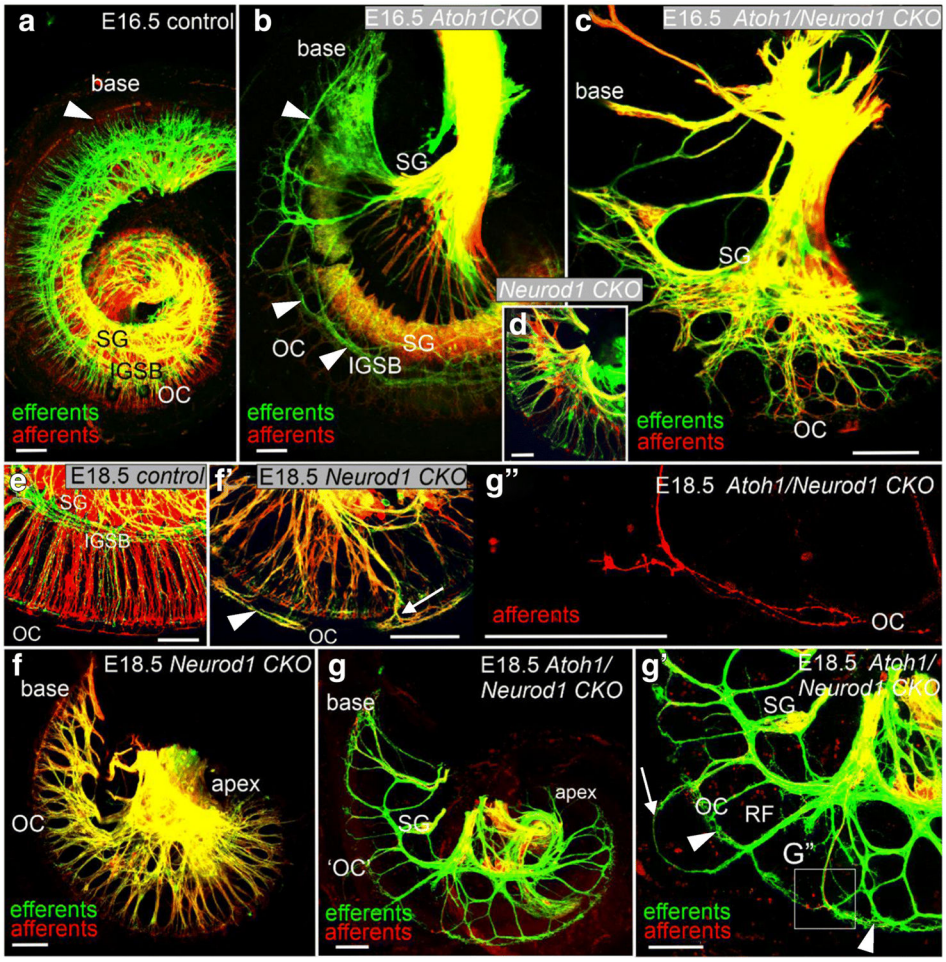

Figure 8. Pattern of organ of Corti innervation is revealed by afferent and efferent tracing from the brain.

The insertions of differently colored dyes into the area of olivocochlear bundle and cochlear nucleus label efferent and afferent fibers in the cochlea. (**A**) In controls, the dye applications overlapped; efferents form the intraganglionic spiral bundle (IGSB); note some afferents extend to OHCs in the base (arrowheads) at E16.5. (**B**) Absent afferent and efferent growth into the region of the organ of Corti (OC) together with missing SG neurons in the base (red) is noticeable in *Atoh1CKO*. Note the formed IGSB on the outer edge of the existing ganglion (arrowheads). (**C**) *Atoh1/Neurod1CKO* shows a larger loss of spiral ganglion neurons than the simple *Atoh1CKO* mutants at E16.5 with tangled network of afferents and efferents. (**D**) Reduced spiral ganglion and disorganized innervation is shown in the *Neurod1CKO* cochlea. (**E-G**) At E18.5, *Neurod1CKO* shows profound and premature outgrowth of afferents to the outer HC region of the OC (arrowhead in F'), the missing IGSB, disorganized radial fibers (RF), and reduced number of SG neurons compared to the control cochlea (E). Note unusual bidirectional afferent projection towards the OC (arrow in F'). A more profound innervation of the area of presumed OC (arrowheads in G') with both afferents and efferents occasionally overshooting (arrow) is found in *Atoh1/Neurod1CKO*. (G") A magnified view of the boxed region (G') shows tracing of a single afferent fiber with

unusual bidirectional projection towards the apex and base in *Atoh1/Neurod1CKO*. Scale bars: 100 μm.

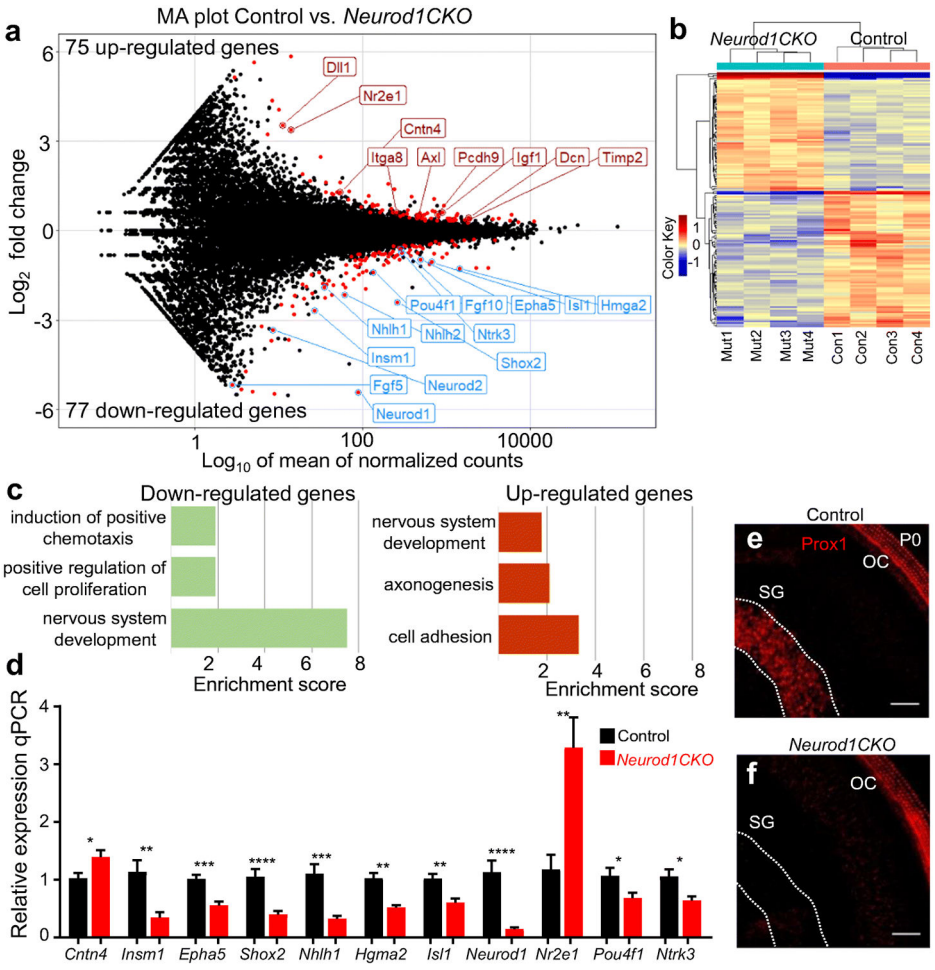

Figure 9. Transcriptome analysis of the inner ear of *Neurod1CKO* vs. controls at E14.5 shows changes in axonogenesis and neurogenesis.

(**A**) MA plot of differentially expressed transcripts (fold change ≥ 30%; adjusted p value < 0.1). (**B**) Heatmap showing hierarchical clustering of downregulated (blue) and upregulated (red) genes in *Neurod1CKO* mutants and controls (n = 4/genotype). (**C**) Gene Ontology (GO) analysis of the differentially expressed genes by David Bioinformatics Resources 6.8 applying a cutoff of Expression Analysis Systematic Explorer (EASE) > 2. Clustering of genes was based on enrichment for biological processes for up-regulated and down-regulated genes. Top three clusters of enriched GO terms in the category biological processes associated with down- and up-regulated genes in *Neurod1CKO* are shown (See also Extended data Tables 10–1, 10–2, 10–3). (**D**) Validation by RT-qPCR of relative expression of selected genes was done using using additional biological samples. The values represent means ± SEM (n = 8/genotype), *t*-test, *P < 0.05, **P < 0.01, ***P < 0.001, ****P < 0.0001. (**E, F**) Transcription factor Prox1 (red) is expressed in supporting cells of the organ of Corti and SG neurons in the control cochlea but no Prox1 is detected in *Neurod1CKO* auditory neurons. The dotted line indicates the boundaries of the SG.

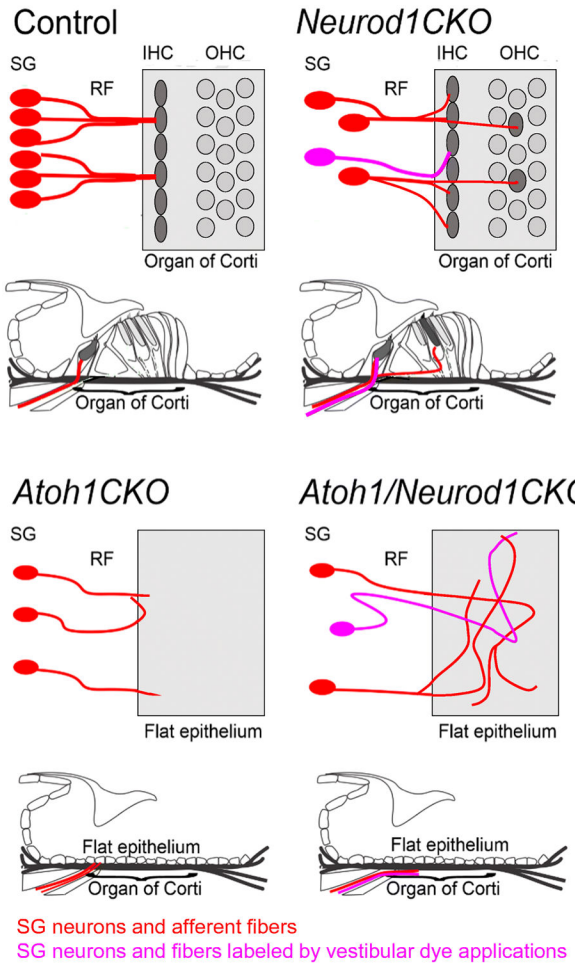

Figure 10. Schematics of structural changes in the cochlea induced by expressional alternations of *Neurod1* and/or *Atoh1* as a combination of cues for guiding neuronal axons to their target sensory organs.

In the control cochlea, spiral ganglion (SG) neurons are radially connected (RF, radial fibers, red) with a single ending to IHC (10–20 neurons/1IHC). The loss of *Atoh1* results in a flat epithelium without any sensory cells and innervation, reduction of SG neurons and retraction of radial fibers. Absence of *Neurod1* correlates with reduced number of SG neurons, a loss of apex-base and vestibular fiber segregation, multiple endings of a single neuron to HCs, and the disorganized epithelium in the apex of *Neurod1CKO*. In *Atoh1/Neurod1CKO* neuronal fibers ramify inside the flat epithelium that replaces the organ of Corti. Magenta color depicts neurons and fibers in the cochlea labeled by the dye application to the vestibular end organs.